RVS®3000 LIDAR PRODUCT FAMILY FROM RENDEZVOUS AND DOCKING APPLICATIONS TO HAZARD MAPPING FOR PLANETARY LANDING

Thomas Kämpfe[(1)], Christoph Schmitt[(1)], Stephan Rhein[(1)], Michael Windmüller[(1)], Rene Pforr[(1)], Michael Schwarz[(1)], Christian Kracht[(1)], Tristan Röll[(1)], Max Möller[(1)]

(1) Jena-Optronik GmbH, Otto-Eppenstein-Straße 3, 07745 Jena, Germany
Phone: +49 3641 200-157, email: thomas.kaempfe@jena-optronik.de

ABSTRACT

Jena-Optronik GmbH's RVS® 3000 is a scanning LiDAR sensor product family, developed for space applications. It has shown its capabilities in rendezvous and docking operations based on retro-reflector tracking in the frame of regular flights to the International Space Station since 2019. This paper presents its continued development, from increasingly demanding docking scenarios towards new applications like planetary landing.
For docking scenarios, the RVS® 3000 was updated with powerful algorithms and hardware for real-time 6 degree-of-freedom (6DOF) pose estimation of uncooperative (no retro reflectors) targets, in the frame of the Mission Extension Vehicle program. Beginning with Artemis III, it shall serve as primary relative navigation sensor on the Orion spacecraft, assuring rendezvous and docking with e.g. Gateway. This requires retro-reflector tracking starting at several kilometers range, down to 6DOF pose estimation of the docking port at close range, for which a detailed CONOPS will be presented.
The increased computation capabilities open up new applications for the RVS® 3000, e.g. illumination independent terrain mapping for Hazard Detection and Avoidance during planetary landing. We show that the RVS® 3000 benefits from the combination of ~1km maximum range with a flexible FoV and a tight beam, allowing envisioning advanced multi-step scan strategies.

1 INTRODUCTION

Scenarios in the discipline of rendezvous and docking between spacecraft continue to require more flexibility from a LiDAR-based navigation sensor, which in the past mostly relied on cooperative targets. Typically, identification of a retro-reflector pattern was used to approach a target vehicle (e.g. for ISS rendezvous). New mission profiles in the field of satellite servicing and space debris removal require docking with targets, which have not been designed for docking or being serviced in-orbit. In such missions, a precise, high-resolution point cloud of an uncooperative target in combination with powerful algorithms and hardware for real-time 6 degree-of-freedom (6DOF) pose estimation enables LiDAR-based relative navigation. This matured and reached the geostationary orbit with the success of Northrop Grumman's (NG) Mission Extension Vehicle (MEV) MEV-1 and MEV-2 in February 2020 and April 2021 [1]. More missions of similar type are in qualification, planned or discussed to date. Future programs such as e.g. Artemis add further complexity to this list, where flexible rendezvous and docking with Gateway [2] is an integral part. Target vehicles can be cooperative (provide reflectors) but might also be non-cooperative (no

reflectors available). Most of them are expected to be equipped with docking ports in compliance with international standards, but there is no guarantee. A second increasingly important application area for LiDARs is terrain mapping for Hazard Detection and Avoidance (HDA) during planetary landing. As with advanced rendezvous and docking, algorithms to efficiently interpret the obtained data play a key role for advanced landing Concept of Operations (CONOPS). Providing advanced calculation capabilities inside the LiDAR permits to optimally use the short time slots available for HDA during the descent. In order to live up to the outlined challenges over the upcoming decades, a precise 3D imaging LiDAR with smart and flexible algorithmic solutions is needed.
The organization of the paper is as follows: We will present the RVS 3000 space LiDAR, its working principle and capabilities. For the first main topic, rendezvous and docking, we will detail the design, test and qualification activities at Jena-Optronik GmbH to demonstrate the suitability of the RVS 3000 product family for all current and potentially upcoming docking missions (including the Artemis program). To this end, heritage and recent developments on the RVS 3000 product family are reviewed shortly. Afterwards the generic design of the LiDAR for the CONOPS against Artemis targets equipped with a docking port as an example is presented, as well as test results gathered with an Engineering Development Unit (EDU). For the second main topic, we will introduce the current developments for Hazard Map Calculation onboard the RVS 3000, detailing the interaction between important parameters of planetary landing scenarios and LiDAR acquisition parameters, leading to a novel multi-step scan algorithm that uses specific advantages of the RVS 3000 to increase the probability of finding a suitable landing spot, allowing a much more flexible design of landing trajectories. Finally we will address the topic of sensor autonomy.

2 THE RVS® 3000 SCANNING LIDAR SENSOR

The RVS 3000 is the successor of Jena-Optronik's legacy RVS sensor, benefitting from the experience of 48 flights to the ISS on the ATV, HTV and Cygnus spacecraft with flawless flight heritage. The RVS 3000 was mainly developed for rendezvous and docking operations, focusing on 2 core functionalities: the detection of retro reflectors, mainly for cooperative targets (e.g. ISS docking port), and the point-cloud based 6DOF object position determination, mainly for uncooperative targets (e.g. satellite servicing). So far, 13 RVS 3000 served in flights to the ISS, and 2 RVS 3000-3D were used by the MEV program, which docked to an uncooperative satellite target in GEO. The algorithm for point cloud based 6DOF target positioning forms the basis for further development of the RVS 3000 towards broader application area, including flexible, cooperative and non-cooperative docking and landing applications. The typical workflow for the LiDAR subsystem is illustrated in Figure 1.

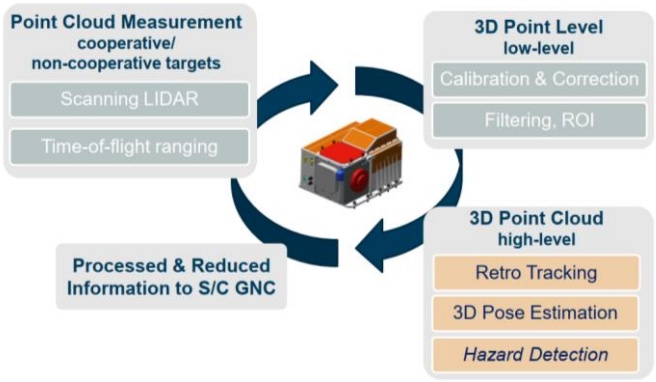

Figure 1. Workflow of a GNC LiDAR subsystem.

The basis is the LiDAR-measured target or surface, resulting in a 3D raw point cloud. Next, low-level data processing yields a high-resolution, precisely calibrated point cloud, followed by high-level analysis such as localization and tracking of retro-reflectors or 6DOF pose estimation by object fitting, extracting the relevant information for the s/c GNC system. Additional functionalities like HDA will be implemented on this level. Depending on the GNC system design, the RVS 3000 can on one hand accept detailed commands for configuring the FoV and scan parameters delivering the point cloud data directly to GNC via e.g. spacewire. On the other hand, the RVS 3000 can serve as a smart and versatile 3D imaging sensor that provides already processed information to s/c GNC, optimizing autonomously its own operational parameters (scan design, laser settings, FoV). This versatility is reflected by the RVS 3000 product family, as detailed in Figure 2.

property	RVS3000	RVS3000-3D	RVS3000-X (L)
general functionality			
use case	cooperative targets	non-cooperative targets	cooperative ***and*** non-cooperative targets, landing application
function	retro tracking JEM-A /JEM-B	6D pose	point cloud ***and/or*** 6D pose / hazard detection
hardware differences and rationale			
IPB (image proc. board)	no IPB	with IPB	without or with IPB
housing thickness		~3 mm	~3 ... 5 mm
rationale	original design	rad. improved, IPB	radiation improved, structural improved multiuse
environment	LEO	LEO / GEO	LEO / GEO
laser			
laser [avg power]	1 laser level	2 discrete laser levels	7 discrete laser levels
power level(s)	< 10 mW	< 10 mW / up to 350 mW	up to 350 mW
data Interface			
interface	MIL	Spacewire / MIL*	Spacewire / (MIL)
qualification status & production			
development status	finished	finished	ongoing
qualification status	TRL 9	TRL 9 / TRL 8 ongoing**	TRL 8 ongoing**
scan parameters			
field of view	40° x 40° ... 1° x 1°	40° x 40° ... 1° x 1°	40° x 40° ... 1° x 1°
operating range - cooperative targets (e.g. retro reflectors) / non-cooperative targets*			
range min; range max	< 1m / --; > 2000 m (3000 m) / --	--/ < 1 m; --/ > 1000 m	< 1m / < 1m; > (3000 m) / > 1000 m
single shot accuracy & precision			
range noise (3Sigma) increasing with range	0.02 m at close range	0.02 m at close range	0.02 m at close range
range bias increasing with range	< 0.02 m at close range	< 0.02 m at close range	< 0.02 m at close range
line-of-sight noise (3 Sigma)	< 0.01 deg	< 0.01 deg	< 0.01 deg
line-of-sight bias	< 0.1 deg	< 0.1 deg	< 0.1 deg
obj. level acc. & prec., POSE estimation (processed information) depends strongly on target geometry			
XYZ noise	< 0.01 cm close range	< 0.02 cm at close range	*point cloud, retro-tracking, 6DPOSE *hazard detection algorithms to be implemented
XYZ bias	< 0.02 cm at close range	< 0.02 cm at close range	
attitude noise (Roll, Pitch,Yaw) (3sigma)	< 0.01 for line-of-sight	< 0.5-1 deg at close range	
attitude bias (Roll, Pitch,Yaw)	< 0.5 at close range	< 0.5 at close range	
power consumption (scan mode @28V), incl. internal heaters			
voltage	28 V	36 V	24 - 32 V
nom. power	62 W	75 W	57/63 W ***
max. power	108 W	121 W	90/97 W ***
mechanical interface			
mass	12,4 kg	13,9 kg	13.6/13.8/15.1/15.3 kg ***
dimensions	342 x 267 x 215 mm³	342 x 267 x 215 mm³	342 x 267 x 215 mm³ 350 x 275 x 220 mm³

legend & remarks	
	( ) expected with adaption of operation parameters & related verification; *depending on optical properties of the target; ** depending on configuration; *** depending on configuration & use of IPB

Figure 2 Datasheets of the RVS®3000 product family

All RVS 3000 versions share a very similar hardware platform, which has been adapted to specific functional and environmental needs of the mission. The most recent development, the RVS 3000-X, is aimed at providing a flexible 3D imaging LiDAR with particular emphasis on an adaptable software and hardware design to allow for various mission types. Several configurations with respect to radiation shielding, calculation power and various interface options enable flexibility, implementing lessons learned from previous missions.

3 RVS® 3000-X – GENERIC DESIGN INTRODUCTION

The application of LiDARs in rendezvous and docking missions can be very diverse. Cooperative targets provide retro reflectors, which tend to produce a strong LiDAR return signal at close range.

The sensor hardware must be able to withstand that return energy without saturation but at the same time provide maximum measurement accuracy to enable docking maneuvers. However, also high maximum range (in the order of a few kilometer) is typically requested from the LiDAR to support precise execution of final burns by the vehicle to initiate the overall rendezvous sequence. This requires maximum sensitivity to detect even very weak return signals. The combination of those two contrary demands drives LiDAR hardware to its limits. Also regarding software, the cooperative target has its challenges. Available retro reflectors need to be extracted from the diffuse background based on measured intensity. Finally robust pattern recognition is applied to identify true reflectors from potential false friends (reflections from windows, MLI, OSR etc). Only if both tasks are executed in perfect symbiosis, the mission can be successful.

Uncooperative targets usually do not provide retro reflectors. Therefore, other techniques have to be applied. The LiDAR system is typically used to generate a 3D point cloud of the target vehicle. Powerful model-based image processing can then be applied to calculate the 6DOF state between chaser and target during their orbital dance. For high 6DOF performance the sensor needs to be able to achieve maximum possible 3D coverage during imaging of the target, again requiring extreme sensitivity, especially since satellite materials can be very LiDAR unfriendly (e.g. Black Kapton or MLI). Uncooperative satellites can also be equipped with very shiny materials such as OSR, that can generate very strong returns similar to reflectors. Thus, the LiDAR needs also in the uncooperative case to be able to master both scenarios: provide high sensitivity and remain performant under the presence of strong return signals.

Based on more than 20 years of experience, Jena-Optronik has developed the RVS 3000-X hardware as latest child of the product family (Figure 2). The goal of this development was on one hand to establish a single hardware configuration, which can support all outlined electronic and optical challenges for a LiDAR in rendezvous and docking, but on the other hand also to design a generic flight software (FSW), which can be re-configured from mission to mission in order to support all currently existing rendezvous and docking needs and targets. Within this chapter the FSW design and algorithms shall be presented. Examples for the hardware and sensing performance are provided later in this paper. The RVS 3000-X is a fully autonomous sensor, selecting scan parameters from scan to scan based on the chosen algorithm and the individual result per frame. The available modes are detailed in the following.

3.1 Single Retro Tracking

This mode is designed for scenarios with a single reflector in the LiDAR FOV, which can be a target vehicle with e.g. a single corner cube, or, in case of a far range cooperative target, multiple retro reflectors that cannot yet be distinguished due to the LiDAR beam divergence, making the reflector group appear as a single “blob”. The LiDAR selects the target object from all visible reflectors as the one closest to the current scan center. FOV size is autonomously adjusted by the FSW to enable maximum performance while maintaining robustness against approach dynamics. Besides real retro reflectors, the LiDAR can also treat or “interpret” other objects in this mode, allowing e.g. far range navigation to a satellite, or a canister within a sample return mission. The available filter options in the RVS 3000-X centroiding algorithm are a powerful tool to guarantee correct target tracking, not just in space, but also during ground testing.

3.2 Retro Pattern Tracking

Cooperative targets often provide reflector patterns for navigation at close range. With at least three reflectors, 6DOF state between the two vehicles can be determined. The RVS 3000-X allows robust tracking of such patterns, applying a Jena-Optronik reflector identification algorithm, based on more than 50 successfully flown ISS dockings in the last 20 years. The LiDAR selects FOV center and size autonomously from scan to scan, where scan parameters are designed by Jena-Optronik for optimal scan density per reflector even during maximum relative dynamics.

3.3 Model-based Pose Estimation

Jena-Optronik has implemented a version of the Iterative Closest Point Algorithm (ICP) in the RVS 3000-X, which is able to calculate 6DOF information via model matching between the target's point cloud and an internal reference deduced from a target CAD model. The algorithm maturity of TRL9 was demonstrated with the successful docking of MEV1 and MEV2, where an RVS®3000-3D (earlier version of RVS 3000-X) served as one of the primary sensors. The ICP algorithm is used to track the target, using previous ICP results to initialize the next scan. For first-scan initialization in rather controlled scenarios (e.g. GEO docking), GNC might have rather good target 6DOF knowledge to seed the LiDAR. Without such knowledge, the RVS 3000-X provides an internal initialization algorithm for a coarse but very quick 6DOF target guess, important for e.g. debris removal or servicing scenarios with tumbling targets. The FSW uses a polygonal aspect hashing algorithm, optimized by Jena-Optronik with AI concepts to support 6DOF pose initialization of targets tumbling with up to several degrees per second. During model-based pose estimation the algorithm result is used by the FSW to define the scan parameters from scan to scan. The LiDAR can be configured to track the complete target vehicle in the scan, or focus on a specific region (region of interest) which can result in better 6DOF performance by its algorithms. FOV Size and Center is autonomously adjusted by the LiDAR from scan to scan based on configuration data engineered by Jena-Optronik for the customer mission.

3.4 Barycenter Tracking

Here, the LiDAR calculates the 3D barycenter of the point cloud, and applies it for FOV adaptation based on a bounding box around the point cloud, providing the 3DOF target position while autonomously adapting the FoV based on the target's visible features. This is useful for e.g. far range satellite tracking down to distances where 6DOF model based pose estimation can be activated.

3.5 "The best of both worlds"

The RVS 3000-X generic design focuses on the interplay of the presented algorithms and modes, which in some scenarios might even run in parallel. For targets of known 3D geometry and additional retro reflectors, the RVS 3000-X can apply reflector identification and model-based pose estimation simultaneously in real-time by calculating two independent 6DOF solutions. The FSW performs cross checks to select the most trustworthy information for control of the next scan window, but can on request also deliver both solutions to GNC. In the following section the docking to an Artemis docking port shall serve as an example, providing test data to visualize how the presented algorithmic solutions master the real world application.

4 RVS® 3000-X – ARTEMIS DOCKING PORT CONOPS

For missions like assembly and later re-supply of the lunar outpost Gateway or lunar lander missions, the Artemis program foresees the use of a docking ports that resemble their twins on the ISS, with slightly changed reflector pattern. However, the CONOPS will remain similar. Figure 3 shows an ISS docking port in compliance with the International Docking System Standard (IDSS) standard (left), outlining its available targets (middle) and how an RVS 3000-X senses it (right). The docking ports provide an external set of 3 corner cubes reflectors (Perimeter Reflector Target - PRT), consisting of 2 hemispherical and 1 planar reflector and designed for far and medium range navigation. Two different patterns equipped with "reflective foil"-based reflectors are available for close range navigation, the Centerline Docking Target (CDT) and Peripheral Docking Target (PDT), designed to be used by laser- or camera-based systems at close range.

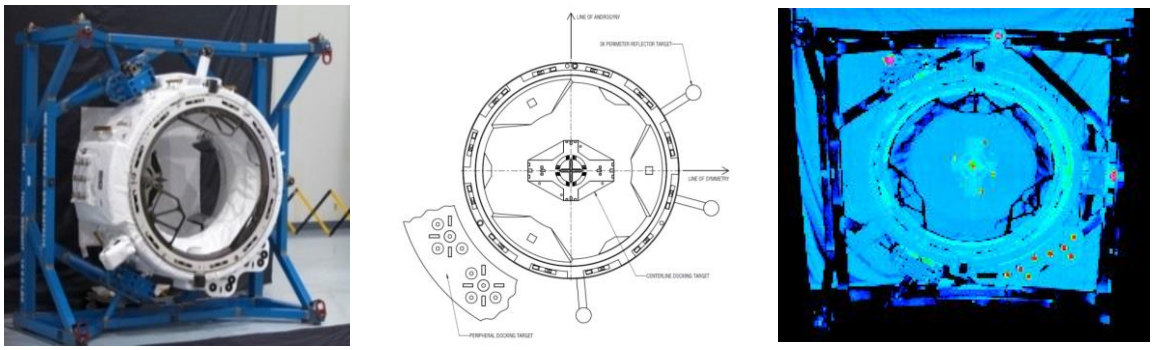

IDA3 FM | IDSS Docking Port | RVS®3000-X High Res Scan

Figure 3. IDSS Docking Port, photo (left), schematic (middle) and LiDAR Scan (right)

The CDT is located inside the docking port and can be used by docking axis co-aligned sensors. Sensors located on the exterior of the chaser spacecraft can use the PDT. This chapter will focus on the usage of CDT by the LiDAR, but it shall be mentioned that all concepts also apply for PDT. The high-level RVS®3000-X LiDAR CONOPS is depicted in Figure 4.

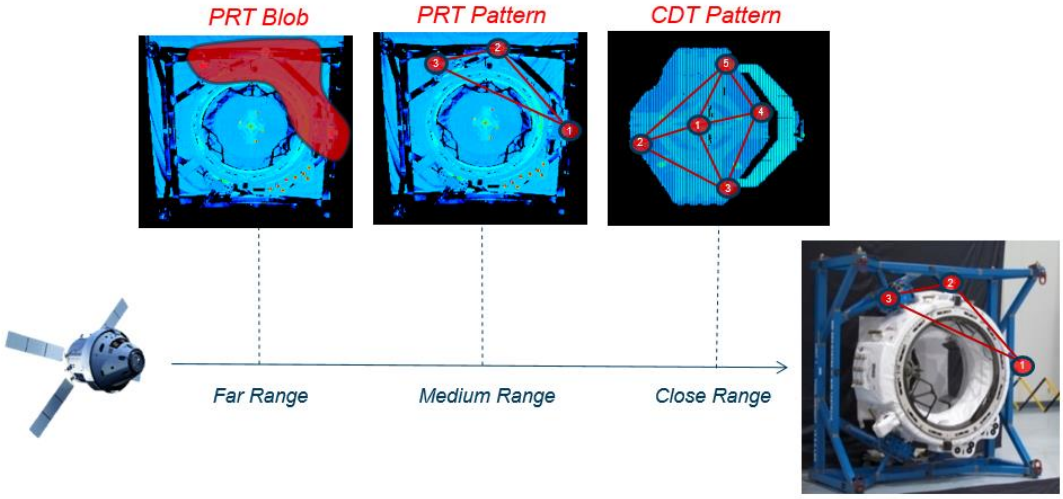

Figure 4. RVS®3000-X LiDAR Concept of Operations (CONOPS) against docking port

The RVS 3000-X is able to acquire the target from >5 km (far range), where the individual reflectors are not distinguishable and perceived as a single “blob”. The RVS 3000-X is operated in Single Reflector Tracking mode as. Approaching medium range (< ≈800m), the LiDAR perceives the PRT as individual reflector objects (centroids), allowing switching to Retro Pattern Tracking mode for pattern recognition on PRT, providing 6DOF information. At close range for final approach, the LiDAR is switched to Retro Pattern Tracking on CDT, using all 5 CDT reflectors simultaneously for calculation of high accuracy 6DOF information. Depending on the LiDARs location on the chaser, PDT can also be selected as final target. For increased robustness and calculation of a dissimilar algorithmic 6DOF solution within the RVS®3000-X box, it can also be switched into Model-based Pose Estimation mode with reflector pattern recognition running in parallel on independent hardware, without interaction. The FSW chooses one 6DOF result for calculation of the next scan window, and provides both results to GNC. This special mode is possible on either the complete docking port (medium range PRT Tracking) or for the final approach at close range (CDT or PDT). Figure 5…8 show some impressions from latest test results.

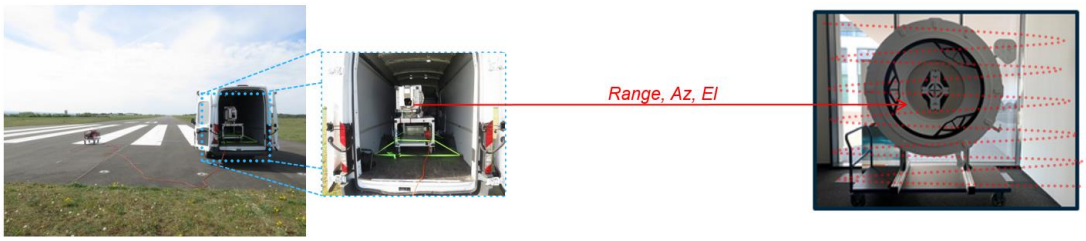

Figure 5. LiDAR Test Setup for runway testing

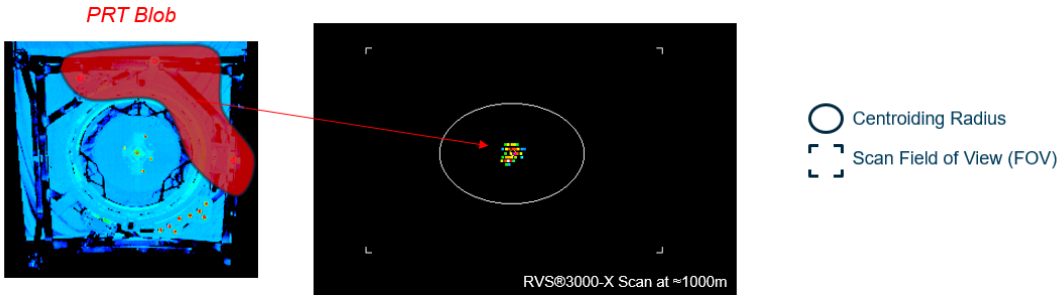

Figure 6. RVS®3000-X – Far Range "Single Retro Tracking" Test Data

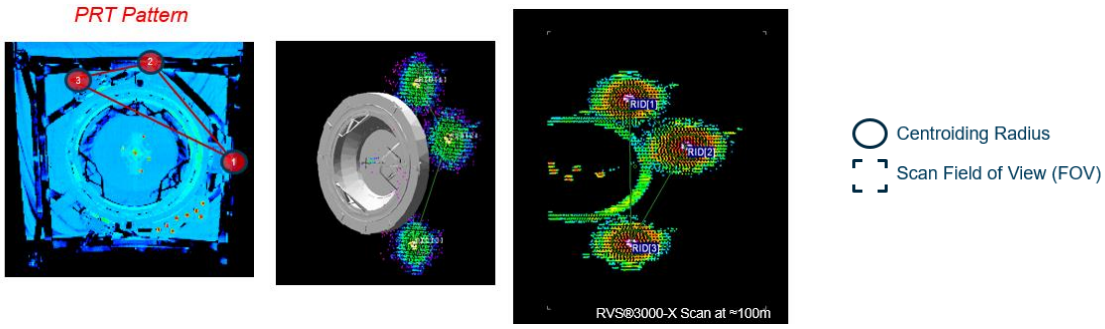

Figure 7. RVS®3000-X – Medium Range "Retro Pattern Tracking" Test Data

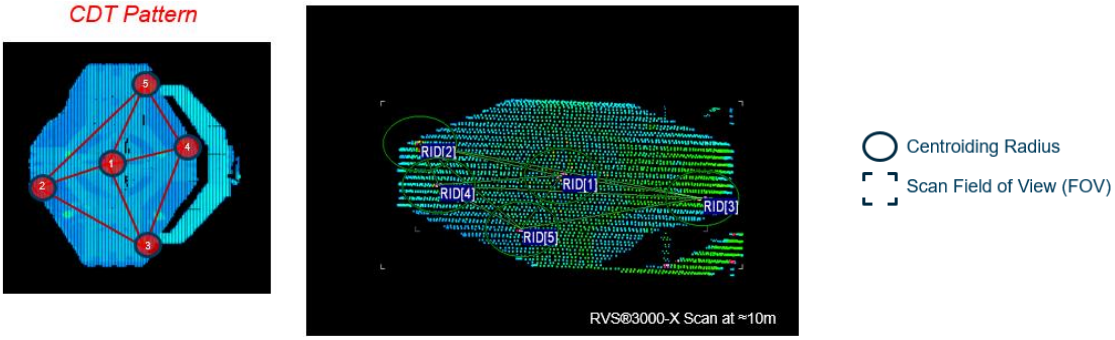

Figure 8. RVS®3000-X – Close Range "Retro Pattern Tracking" Test Data

The shown CONOPS and test data is just one example for the possible applications and use cases of the RVS 3000-X LiDAR. Depending on the customer mission, the FSW can be re-configured without code change, e.g. to serve on the same chaser for docking to Gateway and later after undocking in a follow up mission for pose estimation with a tumbling satellite for debris removal.

Driven by the presented algorithm development and the improved hardware, the last chapter will present a new application area for the RVS 3000: planetary landing.

5 PLANETARY LANDING AND HAZARD DETECTION AND AVOIDANCE (HDA)

Currently, ~50 successful manned and unmanned soft-landing attempts on planetary bodies have been carried out [3], including the Earth, Moon, Venus, Mars, Titan and several asteroids (Eros, Itokawa, Ryugu, Bennu), relying on detailed maps for pre-definition of an inherently safe landing area. As e.g. shown by the Viking landers that touched down just meters away from a ~ 2 m rock (nicknamed "Big Joe" [4]), which would have easily toppled the lander, this approach has its limits. Even with increased resolution and quality of pre-mapping, planets with an atmosphere or volcanic activity can exhibit a changing surface (e.g. rocks sliding down hills, as has been observed by the MRO on Mars [5]). This motivates the use of autonomous landing systems that use a direct, on-the-fly HDA (Hazard Detection and Avoidance) systems to select a safe landing site [6], employing 3D terrain mapping as crucial step. The last decades saw multiple HDA research and development programs by different space agencies, analyzing and proposing different HDA strategies and landing trajectory optimization approaches [8]-[16]. Recently, fully autonomous landing with LiDAR supported on-board HDA was demonstrated by the Chinese Space program's Chang'e 3, 4 and 5 Moon and the Tianwen-1 Mars lander. The conclusion is that LiDAR sensors are an important part of the HDA phase for illumination independent, 3D imaging of the surface. The RVS 3000 offers unique advantages of the scanning LiDAR concept, proposing more flexibility to the planetary landing trajectory design due to improvements in the HDA capabilities. Specifically, the RVS combines a very flexible adaptation of the angular FoV with virtually no dead pixels, a decent maximum range (~1km for moon regolith) and a high resolution (0.45mrad beam). The main drawback of the scanning principle is the point cloud distortion due to lander motion during the scan time, requiring strategies for their mitigation via IMU based pose estimation.

5.1 Planetary landing scenarios and HDA

Figure 9 illustrates an example for a planetary landing trajectory, roughly corresponding to the Chang'e 3 moon landing [11].

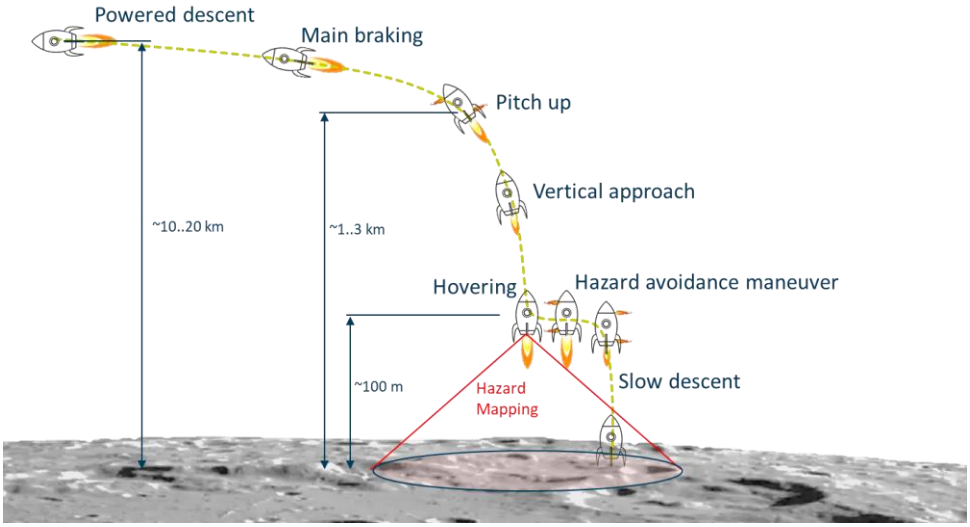

Figure 9. Phases of a typical planetary landing trajectory.

The lander initiates the powered descent at a height of ~10..20 km, guided primarily by camera based terrain relative navigation (TRN). The subsequent braking phase reduces lateral speed, followed by lander pitch-up and transfer to vertical powered descent at about 1..3 km height. At ~100m height HDA is performed, followed by lateral lander displacement according to HDA results. The final slow descent guides the lander to the best landing spot. During HDA, the LiDAR-acquired 3D point cloud has to be transformed into a Cartesian grid based hazard map, usually

characterized by two values: slope and roughness or maximum deviation. Slope indicates the best-fit-plane inclination, and surface roughness or maximum deviation is calculated relative to this fitted plane. Safe landing requires both values to remain below thresholds derived from lander characteristics to avoid tipping or damaging, with typical values of 5…10° for slope and 20…50 cm for roughness or max deviation. Taking both limits into account leads to a scalar merit function indicating lander compatibility. While multiple improvements exist, e.g. advanced plane fitting and slope calculation [10] or multi-level, voxel based analysis [7], we will for the scope of this paper remain with the basic variant of a regular cartesian grid hazard map, plane fit by a least squares algorithm, and vertical maximum deviation relative to this fitted plane.

5.2 LiDAR based HDA

Two principal LiDAR categories exist: scanning LiDARs with a steered laser beam and single detector, and Flash LiDARs with two-dimensional time-of-flight detector arrays. The main advantages of flash-LiDAR systems are mechanical robustness due to the absence of moving parts, and instantaneous image acquisition. Main drawbacks are the fixed and still comparatively low sensor resolution, a much stronger stray light sensitivity, and a maximum range limited to ~100 m to several 100 m. Due to their advantages, flash LiDARs are more and more considered for HDA, meaning that the 3D terrain mapping phase is limited to lower altitudes due to range and resolution limitations. At higher altitudes (~1 km), navigation and early HDA has to rely on camera based imaging and pre-recorded data, meaning that other guidance mechanisms, mainly TRN, based on pre-knowledge from planet-orbiting sensor platforms, have to assure that the potential area for landing, visible to the HDA sensors and attainable by lander guidance at low altitude (~100 m) offers a high probability of including a suitable landing site. As with Neil Armstrong's last-ditch attempt using the last seconds of thruster fuel to find a good spot to land, this can become a close call. It can also limit the flexibility for choosing a landing spot close to interesting areas (concerning geology, surface formations etc..), which becomes more important in recent missions as opposed to the first landings where a successful touchdown was sufficient. To tackle this problem, increasing the altitude of the HDA slot has been proposed, e.g. within NASA's SPLICE project [13], which proposes to scan at 1.0..0.5 km altitude on a ~100m diameter area with a ground resolution in the 5..10 cm range, for which no off-the-shelf LiDAR is currently available [14]. The proposed SPLICE LiDAR prototype connects beam steering with a small detector array to achieve ~MHz point rates, for scanning duration within the 2 sec limit. The FoV is rather limited at 11°.

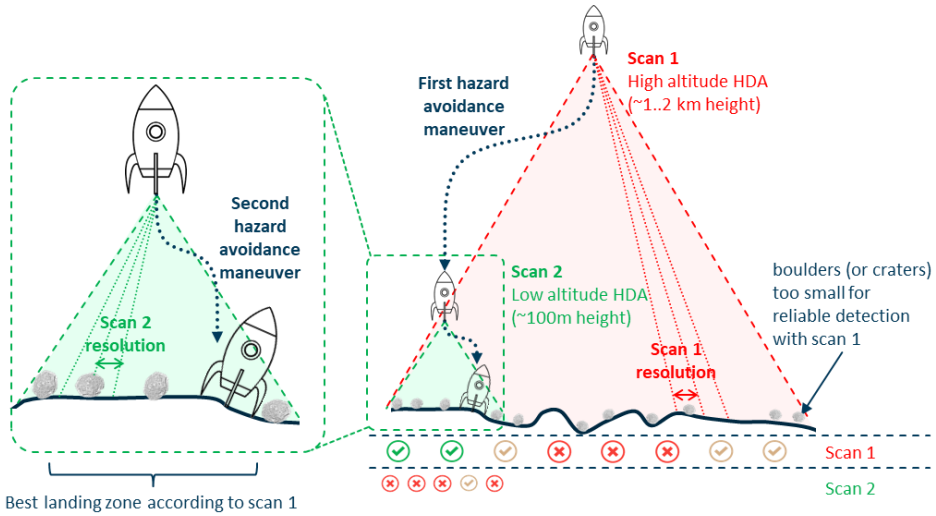

Figure 10. Illustration of low-res high altitude HDA, guiding the lander to a suboptimal region.

Another, more flexible approach is to divide the HDA into two phases (Figure 10). A first HDA

cycle at larger altitudes (some km) already steers the lander away from potentially hazardous areas during the transfer from the braking phase to the vertical descent, whereas the second HDA cycle at lower altitudes (some 100m) assures a suitable landing zone, as evaluated e.g for the ESA Lunar Lander mission [9], or for a potential Mars landing [12]. A common point of these scenarios is the need for a quick (max ~5 sec) 3D scan with high resolution (~ 20 cm) and large FoV (> 30°) at high (~1 km) altitude, leading to ~7 Mpix 3D data, which is not yet possible for flash or scanning LiDAR approach. Flash LiDAR is easily fast enough, but sensor size is still limited to <<100 kpix. Advanced techniques like super resolution allow to get to 0.26 Mpix [15], but require computation intensive processing of multiple frames, taking one to several seconds. The RVS 3000 has a sufficient range of ~1km against moon regolith and provides a very narrow 0.45mrad full divergence beam to resolve ~ 0.5m structures at ~1 km, but requires a very long scan time (~350 sec at 20 kHz pulse repetition frequency for 7 Mpix data). The usefulness of the high altitude HDA approach is therefore at the moment limited when using the common approach of doing one scan of the whole FoV, due to the limited resolution. Assuming a 10 sec scan window for the RVS at ~1 km altitude, and a potential landing region of 500 m lateral size, requiring ~30° FoV, the resulting RVS sampling distance on the ground would be ~2 m. A 100 kpix Flash Lidar would achieve a comparable resolution. This resolution is sufficient for determining dangerous slopes, but will not allow reliable detection of boulders or small craters with the typical maximum acceptable size in the range of 20 to 50 cm. Based on this data, the lander can be trapped in a “rocky plane” scenario during low altitude HDA, where only a much smaller region (typically ~50 m lateral size at 100 m altitude) can be analyzed and attained by HDA maneuvers (Figure 10).

5.3 Scan refinement approach for high altitude HDA

Our proposed solution to improve the reliability of high altitude HDA is to utilize a unique advantage of the scanning LiDAR principle as realized in the RVS 3000: the scanning parameters can be rapidly adapted, allowing a multi scan approach with on the fly scan refinement during one HDA cycle (Figure 11).

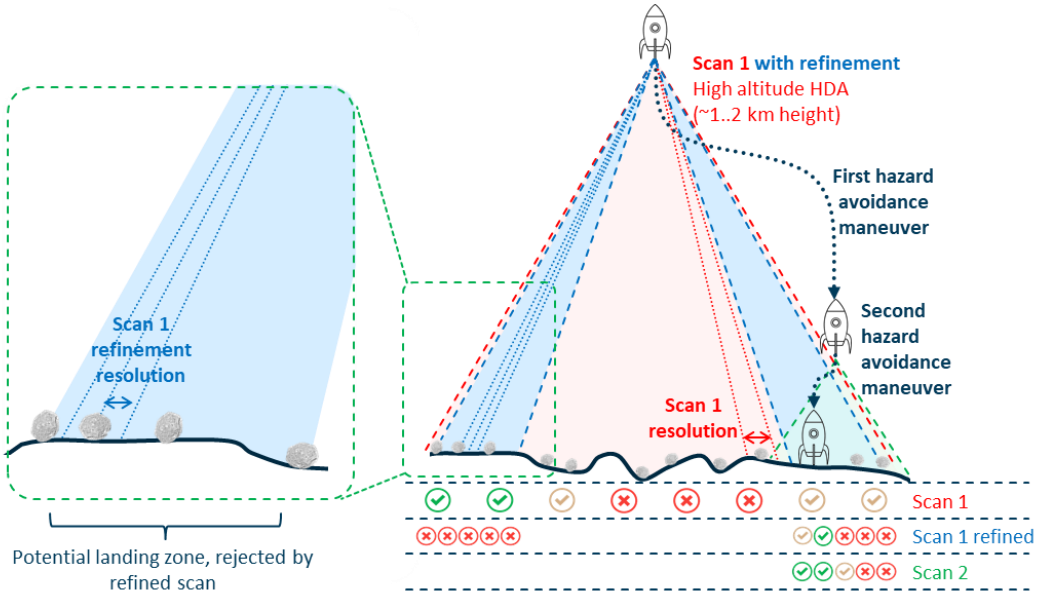

Figure 11. Schematic illustration of a high altitude HDA with refinement scans.

First, a rough scan of the whole potential landing area divides the FoV into patches with slope and roughness information [7]. The main goal is to quickly test the available landing area for large scale hazards (crater ridges, hills, ditches, large scale inclined terrain, etc.), excluding areas from the set of potential landing zones that do not need to be considered in detail. Following this rough scan,

potential landing zones are immediately retested with local, high resolution scans to detect hazardous surface deviations in the 20…50 cm range (boulders, very small craters), greatly reducing the required overall scanning time with regard to a fine scan of the complete FoV while significantly increasing the probability of guiding the lander to a safe zone. Using this two-step scanning regime requires the definition of different sampling distances for rough and fine scans. We propose to use the parameters lander size and landing site tolerance in addition to the minimal tolerable boulder size. A good rule of thumb is to use the lander size as sampling distance for the rough scan, and divide the FoV into patches corresponding to the landing site tolerance. The parameters of the fine scans correspond to the low altitude HDA requiring typically ~20...50 cm resolution. Following guidance by s/c GNC towards the optimal landing zone, the second HDA scan at ~100m height is executed as before (Figure 10).

5.4 Simulation of different Lander Conops using the RVS® 3000 for HDA

In order to test the presented strategies, we implemented a simulation model in Matlab for planetary surface scanning. The moon surface is modeled using PANGU [13], which uses fractal surfaces with added craters and boulders, based on statistical size, age etc. distributions (Figure 12).

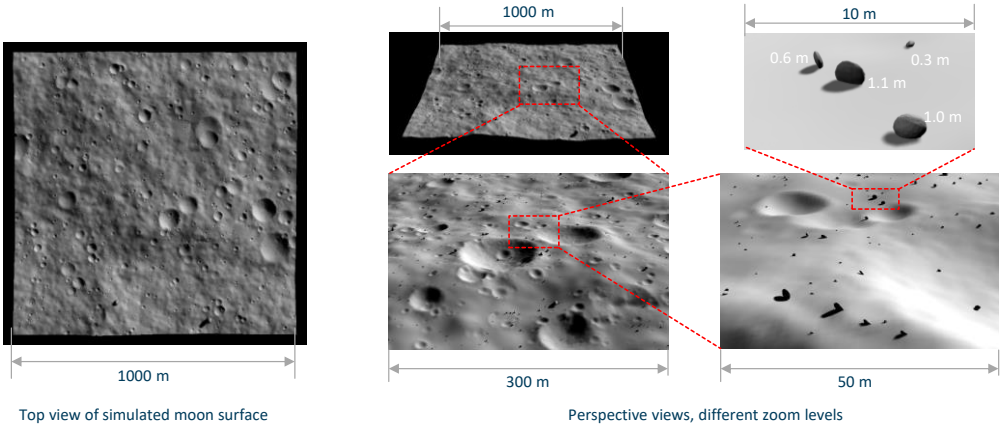

Figure 12. Simulated moon-surface, using Pangu, shown in varying zoom levels.

Typical parameter sets for representative moon surfaces are used, adapted to create challenging cases with a limited amount of good landing spots. Figure 12 shows an example of a 1000 m^2 moon surface, showing large scale surface undulations in the 100 m range as well as fine details down to the sub-meter range. The numerical simulations are carried out using a raytracing-based LiDAR simulation integrated in Pangu, where the divergence is simulated by sending out a ray bundle within the 1/e² beam divergence, and using the first returned signal for range detection (including a more complete RVS simulation modules available at Jena-Optronik, taking surface reflectivity, RVS receiver optics, power threshold etc. correctly into account, is in development). Each point cloud entry is then attributed to a cartesian grid of hazard map patches (Figure 13), resulting in a slope value α and height deviation δ for each patch. The merit value m is then calculated according to Eq. 1. using lander specific limits for α_{max} and δ_{max}.

$$m = \begin{cases} 1 & for\ \alpha > \alpha_{max} \\ 1 & for\ \delta > \delta_{max} \\ 0.5\left(\frac{\alpha}{\alpha_{max}} + \frac{\delta}{\delta_{max}}\right) & for\ all\ other\ cases \end{cases} \quad (1)$$

The resulting value is 0 for a perfectly flat surface and increases for increasing slope and deviation, reaching 1 when one or both maximum values have been violated. m is then used to order the patches according to their adequacy for landing.

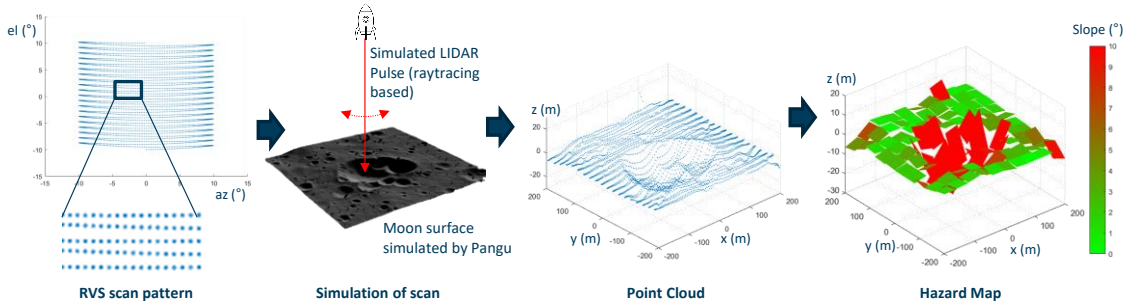

Figure 13. Simulation workflow for simulating the LiDAR response and calculating a hazard map

Lander motion and rotation are not yet taken into account. We assume a first HDA scan window with a hovering, stationary lander at 1 km altitude, guiding the lander to the optimal landing zone, where at 100 m height a second HDA scan is performed, allowing for a final correction. For comparability, the two approaches are configured for using approximately the same scan time for the 1st scan at 1000 m altitude. Assuming a window of ~10 sec for scanning, data transfer and computing, we chose a 6.5 sec scan time limitation. The FoV is chosen to be 30° x 30°, allowing to investigate a landing area of ~540 m x 540 m.

Approach A – one complete-FoV high altitude scan: The scan uses its complete time slot of 6.5 s, which results for the RVS specific scan pattern in a maximum spot separation on ground of ~2.5m, roughly comparable to a 100 kpix flash LiDAR. The scan is evaluated on 20 x 20 patches of ~27 m x 27 m size each, obtaining *m* as described in Eq. 1 (visualized in Figure 14, top row).

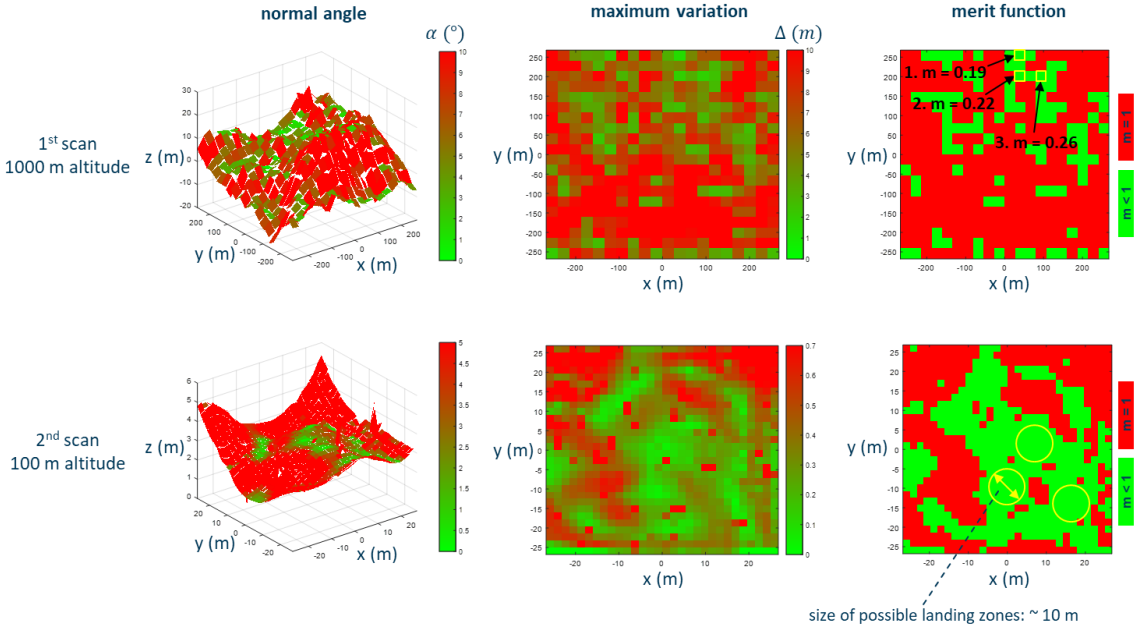

Figure 14. Hazard Map results for approach A, using a single, long high altitude scan

The patch with the lowest merit value of m = 0.19 is chosen (Figure 14, top right) for the 2nd HDA scan at 100 m altitude. FoV is then set to ~50 x 50 m as available lander guidance range, and a 4 s scan window is attributed to the 2nd HDA phase, resulting in a maximum scan point separation of ~ 30 cm. The resulting hazard map (Figure 14, lower row) shows several localized peaks due to the presence of obstacles such as boulders. Assuming α_{max} = 5° and δ_{max} = 0.5 m, the size of a possible landing zone is around 10 m (Figure 14, bottom row).

Approach B - shorter high altitude scan, followed by refinement scans: Using the same

parameter as for approach A, the scan of the complete FoV is shortened to 1.5 sec, resulting in a larger maximum scan point separation of ~5.4 m. The hazard maps change only slightly (Figure 15, top row), but the *m*-value classified optimal patches remain in the same overall area.

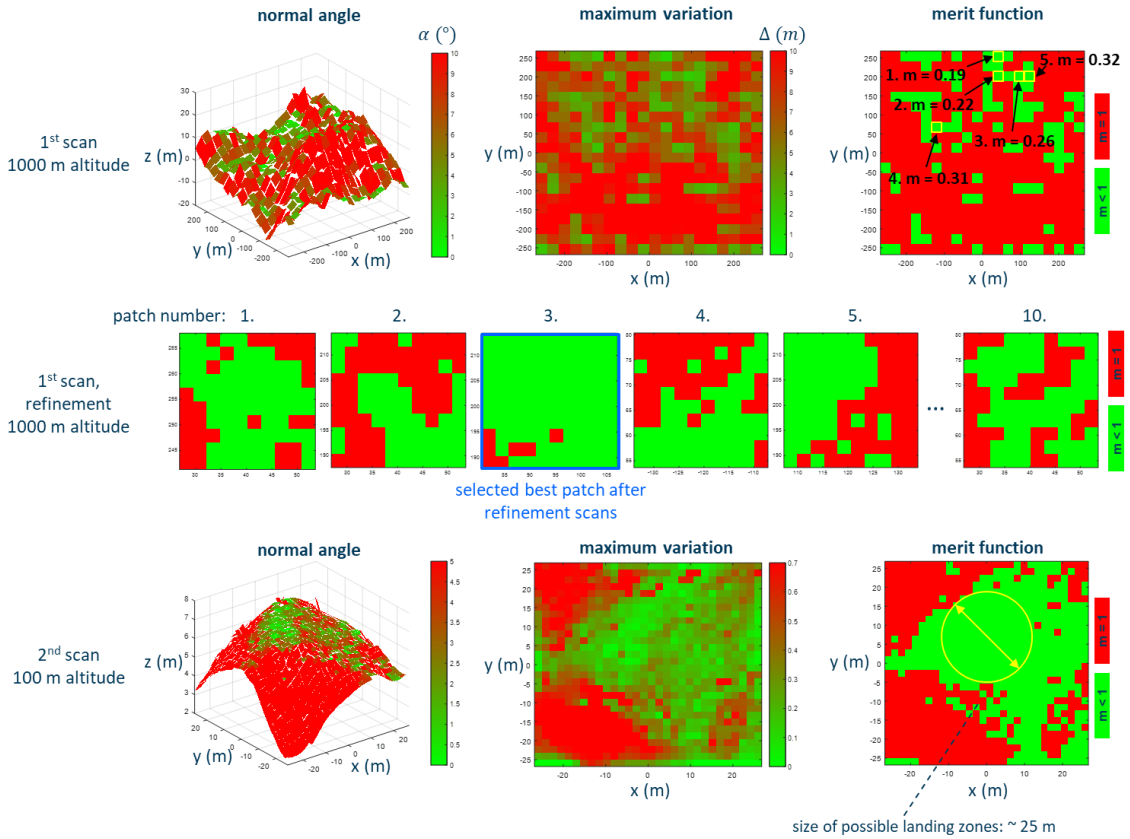

Figure 15. Hazard Map results for approach B, using high altitude refinement scans

The remaining time is now used to do localized rescans with optimized resolution. The number of rescan patches is determined by the beam divergence of 0.45mrad full angle = 45cm spot size on ground for 1 km height, and optimizing the scan pattern for 45 cm maximal spot separation, which can be achieved by a 0.5 s scan on each ~26 m x 26 m patch, thus the 10 patches with the lowest *m*-value can be scanned in the remaining 5s. The *m*-value is analyzed on a 10 x 10 hazard map grid (Figure 15, middle row). The best patch is chosen by analyzing the largest connected area of merit value < 1 inside the refinement scans, resulting in a guidance to patch 3 for the 100 m altitude hold point, where the second HDA cycle is done with the same parameters as for approach A (Figure 15, bottom row). The possible landing zone for approach B is notably larger, ~25 m in diameter. To have a better visual understanding, Figure 16 shows 3D renders in top-down and perspective view of the choices of landing zones for the two different approaches,.

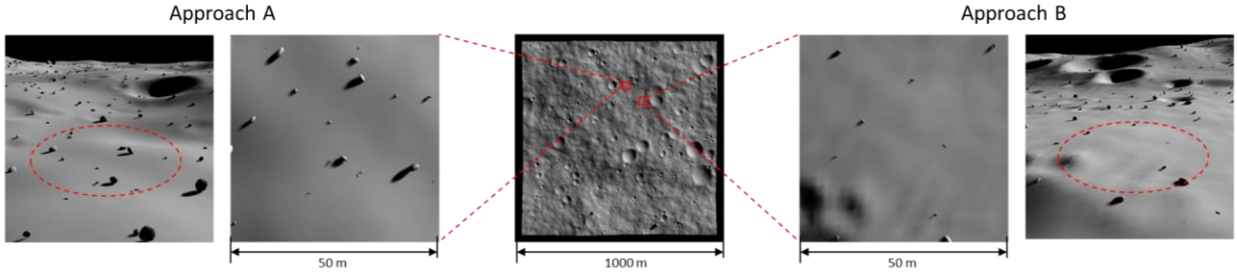

Figure 16. Chosen landing zones for Approach A (left) and B (right)

As expected, both approaches chose areas free of large scale hazards (craters, hills..) easily

resolvable at 1 km height. The problem of Approach A is evident by the presence of boulders that are in a size range of one to several meters, thus typically dangerous for landers, but not detectable for the large altitude HDA scan. Approach B's site is to a much larger degree free of such hazards.

5.5 Sensor Autonomy in Planetary Landing Applications

In order to implement the outlined HDA strategies for planetary landing, an important question is the level sensor autonomy (Figure 17). The RVS 3000 is currently being developed towards implementing higher level algorithms, if required by the overall mission design.

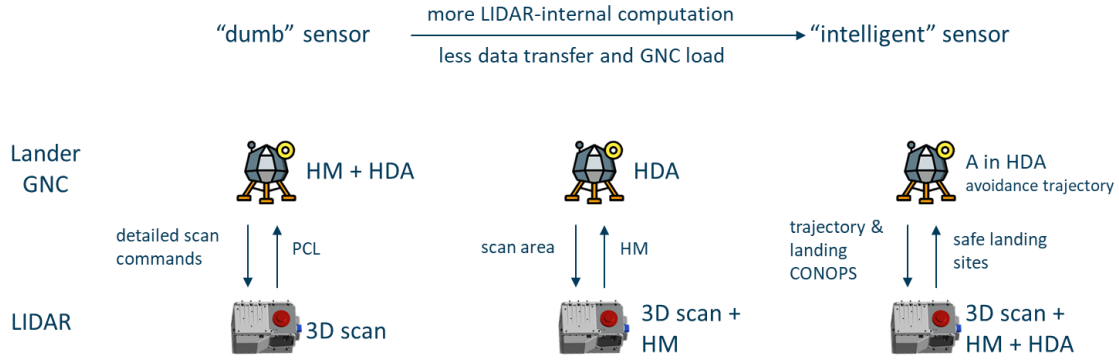

Figure 17. Illustration of autonomy levels for Hazard Map (HM) Generation in HDA applications

The currently completely TRL9 space-qualified variant of the RVS 3000 supports the lowest level of autonomy (Figure 17, left) via its manual scan mode, allowing s/c GNC to freely parametrize the scan, start it, and receive the obtained point cloud, with all further HDA activities done in GNC, allowing for data fusion with other sensors, and to keep complete control over the algorithms. However, the advantages of the multi-step refinement-scan approach cannot be fully exploited due to the RVS has to wait for new s/c GNC TC's. To improve on this, medium and high autonomy levels (Figure 17, middle and right) are currently in development, based on a dedicated PCB with the same RTG4™ FPGA that powers 6DOF pose determination in docking applications. An important goal is a tight connection between data acquisition, algorithms and scan refinement, using the architecture of the RTG4 to massively parallelize the hazard map patch calculation. Additionally, with RVS-internal data treatment each patch calculation can start as soon as all corresponding points have been acquired, minimizing lag time between the LiDAR scan and HDA transfer to GNC. The advantage of a smarter sensor besides speed could be to help mitigating risk, by providing raw data to GNC as well as an independent suggestion for preferable landing sites.

5.6 Preliminary landing scenario tests of the RVS® 3000

Preliminary tests to estimate the capability of the RVS for 3D terrain mapping in lander applications have been carried out, using small scale moon-mockups, and analyzing the obtained point cloud. The mockup was measured on an airfield, allowing tests up to ~1 km range (see Figure 18).

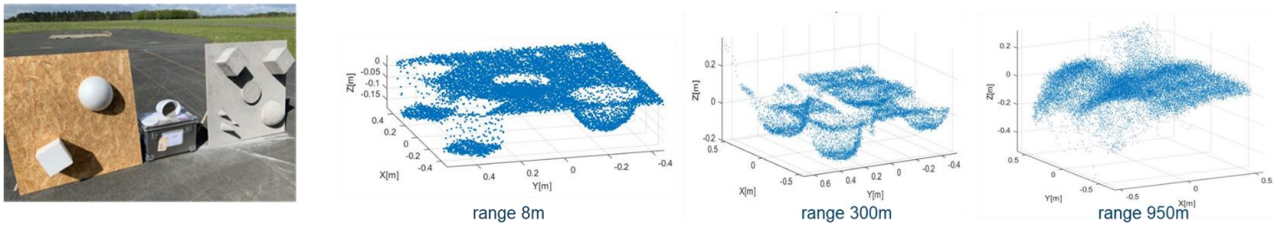

Figure 18. Point clouds (right) for different ranges to a moon mockup (left), installed on an airfield

These tests were not yet done using typical planetary landing CONOPS, so the obtained point clouds are not completely representative (longer scan times). However, they confirmed that the

RVS' optical resolution and noise behavior in principle allows detecting structures of sizes down to ~20 cm up to 950 m range, validating the feasibility of the proposed approaches. More systematic studies are planned, taking the findings from the preceding sections into account.

6 CONCLUSION

The RVS 3000 product family of scanning LIDARs was presented, showing its high performance retro reflector identification, autonomous 6DOF pose estimation, and, in general, high resolution 3D imaging capability. The RVS 3000-X is very flexible in hardware and software, as shown with the tracking and docking CONOPS within the Artemis program. We also presented a novel approach for planetary landing HDA using multi-step refinement scans. We plan to further develop the RVS 3000 towards a higher autonomy, allowing to better optimize the CONOPS with respect to tracking, docking, or landing, freeing the s/c GNC from significant workload. Current developments focus also on improving key parameters of the RVS: increased pulse rate (towards 40…80 kHz), flexibly adaptable FoV outline (e.g. ellipse) and scan point distribution (Cartesian grid). In summary, the RVS development activities at Jena-Optronik rest on two pillars: providing a sophisticated space qualified HW platform for obtaining optimally adapted 3D point-clouds, and collaborating with s/c GNC developers to advance the implemented algorithms, deciding together how to best configure the autonomy level and computation capabilities of the LiDAR for a specific mission.

7 REFERENCES

[1] N. T. Redd, "Bringing satellites back from the dead: Mission extension vehicles give defunct spacecraft a new lease on life", *IEEE Spectrum*, vol. 57, no. 8, pp. 6-7, Aug. 2020.
[2] B. Dunbar, Gateway https://www.nasa.gov/gateway, (accessed 22 May 2023).
[3] Woicke, S. "Hazard Relative Navigation - Towards Safe Autonomous Planetary Landings in Unknown Terrain," Thesis, 2019.
[4] Manning, R. M., & Adler, M. (2005, September). Landing on Mars. In *AIAA Space 2005*.
[5] Malin, M. C. "Context Camera Investigation on Board the Mars Reconnaissance Orbiter." *J. Geophys. Res* 112 (2007): E05S04.
[6] Brady, T. and Paschall, S. "The Challenge of Safe Lunar Landing.", *2010 IEEE Aerospace Conference*, 1–14, 2010.
[7] Mango, D., Opromolla, R. and Schmitt, C. "Hazard Detection and Landing Site Selection for Planetary Exploration Using LiDAR." *2020 IEEE 7th International Workshop on Metrology for AeroSpace (MetroAeroSpace)*, 392–97. IEEE, 2020.
[8] Johnson, Andrew E., Andres Huertas, Robert A. Werner, and James F. Montgomery. "Analysis of On-Board Hazard Detection and Avoidance for Safe Lunar Landing." *2008 IEEE Aerospace Conference*, 1–9. IEEE, 2008.
[9] Roback, V., Bulyshev, A., Amzajerdian, F. and Reisse, R. "Helicopter Flight Test of 3-D Imaging Flash LiDAR Technology for Safe, Autonomous, and Precise Planetary Landing." *SPIE Defense, Security, and Sensing*, Vol. 8731, 2013.
[10] Xiao, Xueming, Hutao Cui, and Yang Tian. "Robust Plane Fitting Algorithm for Landing Hazard Detection." *IEEE Transactions on Aerospace and Electronic Systems* 51 (October 1, 2015): 2864–75. https://doi.org/10.1109/TAES.2015.140378.
[11] Kanani, K. et al. "Sensor Data Fusion For Hazard Mapping And Piloting," *13th International Planetary Probe Workshop* 2016.
[12] Xiao, Xueming, Meibao Yao, Hutao Cui, and Yuegang Fu. "Safe Mars Landing Strategy: Towards Lidar-Based High Altitude Hazard Detection." *Advances in Space Research* 63, no. 8 (April 15, 2019): 2535–50. https://doi.org/10.1016/j.asr.2019.01.005.
[13] Restrepo, C.I. et al., "Next-Generation Nasa Hazard Detection System Development." *AIAA Scitech 2020 Forum*, 0368, 2020.
[14] Carson, J. et al., "Precise and Safe Landing Navigation Technologies for Solar System Exploration" Planetary Science and *Astrobiology Decadal Survey* 53 (May 1, 2021): 413. https://doi.org/10.3847/25c2cfeb.7f40f610.
[15] Amzajerdian, F. et al., "Performance of Flash Lidar with Real-Time Image Enhancement Algorithm for Landing Hazard Avoidance." *AIAA SCITECH 2022 Forum*, 2206, 2022.
[16] Wu, Bo, Jie Dong, Yiran Wang, Wei Rao, Zezhou Sun, Zhaojin Li, Zhiyun Tan, et al. "Landing Site Selection and Characterisation of Tianwen-1 (Zhurong Rover) on Mars." *Journal of Geophysical Research: Planets* 127 (April 1, 2022).

8 ACKNOWLEDGEMENT

The analysis presented in this paper has been partially performed under the ESA activity "LiDAR hazard map algorithms for planetary landing" (contract 4000136431/21/NL/MGu). Jena-Optronik acknowledges the collaboration with Leo Novelli and Steeve Kowaltschek.